ELSEVIER

Bone 39 (2006) 434–442

BONE

www.elsevier.com/locate/bone

Raman spectroscopic evidence for octacalcium phosphate and other transient mineral species deposited during intramembranous mineralization

Nicole J. Crane [a], Victoria Popescu [a], Michael D. Morris [a,*], Pieter Steenhuis [b], Michael A. Ignelzi Jr. [b]

[a] *Department of Chemistry, University of Michigan, Ann Arbor, MI 48109-1055, USA*
[b] *Department of Orthodontics and Pediatric Dentistry, University of Michigan School of Dentistry, Ann Arbor, MI 48109-1078, USA*

Received 14 December 2005; revised 14 February 2006; accepted 21 February 2006
Available online 19 April 2006

Abstract

To understand early mineralization events, we studied living murine calvarial tissue by Raman spectroscopy using fibroblast growth factor 2 (FGF2)-soaked porous beads. We detected increased levels of a transient phase resembling octacalcium phosphate in sutures undergoing premature suture closure.

Introduction: Several calcium phosphates have been postulated as the earliest inorganic precursors to bone mineral. They are unstable and have not been previously detected in tissue specimens. Whether the same intermediates are formed in sutures undergoing premature closure is also unknown.

Methods: Six coronal suture tissue specimens from fetal day 18.5 B6CBA F_1/J wild-type mice were studied. Three sutures specimens were treated with FGF2-soaked heparin acrylic beads to induce accelerated mineralization and premature suture closure. Three control specimens were treated with empty heparin acrylic beads. All sutures were maintained as organ cultures to permit repeated spectral analyses at 12–24 h intervals over a 72-h period.

Results: During the first 24 h, the spectra contained bands of octacalcium phosphate (OCP) or an OCP-like mineral. The main phosphorus–oxygen stretch was at 955 cm^{-1}, instead of the 957–959 cm^{-1} seen in bone mineral, and there was an additional band at 1010–1014 cm^{-1}, as expected for OCP. A broad band was found at 945 cm^{-1}, characteristic of a highly disordered or amorphous calcium phosphate. An increased amount of mineral was observed in FGF2-treated sutures, but no qualitative differences in Raman spectra were observed between experimental and control specimens.

Conclusions: Inorganic mineral deposition proceeds through transient intermediates, including an OCP-like phase. Although this transient phase has been observed in purely inorganic model systems, this study is the first to report OCP or an OCP-like intermediate in living tissue. Raman microspectroscopy allows observation of this transient mineral and may allow observation of other precursors as well.

Keywords: Bone; Mineralization; Fibroblast growth factor (FGF2); Octacalcium phosphate (OCP); Raman microspectroscopy

Introduction

It is widely accepted that, in many, if not all, cases, biomineralization proceeds through a series of intermediates beginning with amorphous precipitates and hydrated crystallites and proceeding to the stable form [1]. Proteins are involved at every stage of the biomineralization process, especially in guiding crystallite growth in preferred directions. This view has been concisely stated, and the evidence summarized recently [1]. Many studies have confirmed this general pathway in invertebrates. Surprisingly, mammalian bone is one tissue for which this general pathway has not been fully elucidated. Many years ago, it was suggested that a progression of mineral phases should occur in bone tissue as well [2]. More than 30 years ago, in vitro room temperature studies showed a progression at pH 7.4 from an amorphous calcium phosphate to a mineral similar to octacalcium phosphate (OCP) over a 24-h period [3].

* Corresponding author. Fax: +1 734 615 3790.
E-mail addresses: cranen@niddk.nih.gov (N.J. Crane), vpopescu@umich.edu (V. Popescu), mdmorris@umich.edu (M.D. Morris), psteenhu@umich.edu (P. Steenhuis), ignelzi@umich.edu (M.A. Ignelzi).

8756-3282/$ - see front matter © 2006 Elsevier Inc. All rights reserved.
doi:10.1016/j.bone.2006.02.059

By the middle 1989, Brown and co-workers were summarizing their view that OCP was the unstable precursor to the carbonated apatite of both tooth and bone mineral, although there was no direct evidence for OCP participation. These workers pointed the many structural similarities between OCP and both dahllite and hydroxyapatite (HAP) and, in particular, the existence in OCP of a hydrated layer that could be the locus of interaction with solution constituents [4]. Lowenstam and Weiner [5] did show that in chitons formation of tooth mineral begins with disordered calcium phosphate (ACP) which is slowly converted to the dahllite structure of the mature tooth mineral. Even now, there is little direct evidence for the participation of transient mineral phases in bone mineralization.

In chick bud mesenchymal and osteoblast mineralizing cell cultures, the only mineral found was a poorly crystalline apatite [6]. In a follow-up study, no bands were observed for precursors of bone apatite, although octacalcium phosphate (OCP) was sought [7]. However, Sauer and Wuthier report that, in matrix vesicles (MVs), the first distinct mineral phase to form contained acidic phosphate bands [8]. The mineral phase present in fully mineralized MVs was much more apatitic. These findings are consistent with the formation of an OCP-like precursor during MVs mineral formation that subsequently hydrolyzes to form hydroxyapatite [9].

OCP has long been known to be thermodynamically unstable with respect to hydroxyapatite [10]. Although OCP was proposed in tooth enamel [2,4], it has been thought that detection of OCP in bone is possible only if some matrix constituent is inhibiting formation of the final stable apatite. OCP formation is affected by several solution factors including calcium ion concentration, total ionic phosphate concentration PO_4 and Ca/PO_4 ratio, pH and presence of phosphoproteins and of small amounts of fluoride (F^-) ions. Study of precipitation of calcium phosphates in serum revealed that OCP was formed at first and then hydrolyzed to a more basic form, OCPH (octacalcium phosphate hydrolyzate), but never reached the solubility of hydroxyapatite [4]. In a constant pH inorganic system, OCP was found to precipitate only when the initial Ca^{2+}/PO_4 ratio was low. At pH ~7.4, OCP crystals grew on amelogenin as plate-like crystallites and fine needles with the *c* axis predominantly parallel to the fibrial axis of the protein. The crystallites in the matrix were almost 100 times smaller than those that grew outside [11].

Other minerals have also been detected under unusual conditions. Chaudhary and co-workers proposed an amorphous calcium phosphate loosely bound to the matrix in bone marrow stromal cells treated with fibroblast growth factor 2 (FGF2) alone [12]. We have found traces of a mineral spectroscopically similar to β-tricalcium phosphate (β-TCP) in cell cultures, where a large excess of β-triglycerophosphate (β-GP) caused early cell death and halted mineralization prior to conversion to an apatitic lattice [13].

Our hypothesis is that the first precipitated inorganics are monohydrogen-phosphate-rich calcium salts, including an OCP-like phase. Monohydrogen phosphate incorporation is expected because physiological pH ca. 7.4 is quite close to pK_2 of phosphoric acid, 7.21 at 25°C. To test this hypothesis, we use Raman spectroscopy to follow the mineralization of control and FGF2-treated murine calvarial organ cultures over 72-h periods under conditions that preserve tissue viability. We have found previously that there is increased fusion in mice calvaria when treated with FGF1, 2, 4 and 9 and that FGF2 treatment elicited the greatest response [14].

It has been difficult to test hypotheses about the presence of transient inorganic phases in bone mineralization. Many of the standard techniques for elucidating mineral composition and crystal structure cannot be used in living tissue. Most are limited in their applicability to water-containing specimens, and most require large amounts of material. Scanning electron microscopy (SEM), X-ray diffraction (XRD), solid-state nuclear magnetic resonance spectroscopy (NMR) and Fourier transform infrared spectroscopy (FTIR) require extensive specimen pre-treatment that makes application to unstable species difficult or impossible. While it might prove possible to use FTIR in the attenuated total reflection mode on fresh tissue specimens, the requirement for physical contact complicates the experiment, especially if mapping is required. All of these methods are conventionally applied to bone tissue specimens that have been embedded and sectioned or otherwise extensively prepared for examination or to the products of cell cultures that have been similarly treated [6,13,15–18]. In every case, mineralization and metabolic processes are stopped before any examination takes place. Short-lived intermediates can be converted to stable minerals during the minutes or hours that elapse before measurement.

Raman microspectroscopy is well suited for the study of living tissue. It provides similar composition and chemical structure information to that of FTIR microspectroscopy, but with 0.5–2 μm lateral resolution. It can be used for either thick or thin specimens that can be fresh or fixed and embedded. Most importantly, Raman spectroscopy is readily applied to hydrated tissue specimens because water is a weak Raman scatterer and because the constituents of most buffers and cell culture media are sufficiently dilute that their Raman spectra are near or below the detection limits of the technique and if not can easily be resolved from the spectra of bone tissue components. Spectra are observable through glass and fused silica, facilitating measurement in standard Petri dishes or plastic Petri dishes with silica windows. There have been several studies of the Raman spectra of inorganic calcium phosphates relevant to bone mineral chemistry. Fowler and co-workers have presented Raman and infrared spectra of OCP and related compounds and have made band assignments on the basis of these studies [19]. Sauer and co-workers have surveyed the Raman spectra of several synthetic calcium phosphates, including OCP, as well as phosphate mineral in matrix vesicles [9]. Their less detailed OCP assignments generally agree with those of Fowler et al. Our group has reviewed the infrared and Raman spectroscopy of mineralized tissue [20].

Using Raman spectroscopy, we have already shown that an FGF2 treatment leads to premature closure of the murine calvarial suture, increasing the rate of the mineral deposition, but not the structure of the mineral itself [14,21–24]. FGFR2 signaling is thought to be essential for osteogenic cell

differentiation and proliferation during the process of suture growth and closure because FGFR2 transcripts are expressed at the osteogenic fronts in developing calvaria bone [25]. Our previous work suggests that models for craniosynostosis can be useful in the study of the normal mineralization process and may complement recent solid-state ^{31}P NMR work identifying protein and phosphorylated protein complexes containing inorganic phosphate ions that may be immediate precursors to mineral crystallites [26].

That there may be unstable mineral precursors to carbonated apatites suggests that it would be useful to study changes in living tissue as mineralization proceeds in order to find and identify transient intermediates formed under physiological and pathological conditions. Time studies of living tissue specimens could also reduce the number of animals needed for statistically valid results. Instead of sacrificing several animals to obtain data for each time point, the time evolution of several tissue specimens could be followed over an extended period. Such experiments might be generally useful in tissue mineralization studies and might resolve ambiguities that arise from the variation between different tissue specimens at the same time points. Therefore, we have followed the mineralization of control and FGF2-treated murine organ cultures over a 72-h period under conditions that preserve tissue viability.

Materials and methods

Raman tissue culture cell construction

To allow spectroscopic observation of tissue, 18-mm diameter, 0.17-mm-thick fused silica cover slips (Esco Products, Oak Ridge, NJ) were cemented into openings drilled through 50-mm diameter polystyrene Petri dish covers. Into each Petri dish, a septum (Alltech Associates, Deerfield, IL) was cemented to allow introduction of culture media without perturbation to the system. To raise them near to the fused silica viewing window, calvaria were placed on fused silica flats, using a Viton O-ring under the flats as needed to position the specimens. The silica coverslip, septum, O-ring and silica platform were secured with epoxy cement (3M, St. Paul, MN), which was allowed to dry overnight in an oven at 37°C. After drying, a piece of Parafilm was placed around the perimeter of the bottom piece of the Petri dish to ensure a tight but gas-permeable seal. Prior to introduction of the sample, the bottom and top of the modified Petri dishes were sterilized by ethanol treatment and UV irradiation in a laminar flow hood to prevent contamination.

Calvaria organ culture and application of FGF2-soaked beads

We followed previously described protocols [14]. Six B6CBA F_1/J wild-type mouse calvaria were dissected at fetal day 18.5 (F18.5), and coronal sutures were isolated. The explants were triangular with a base of ~1.5–2 mm and a height of 2.5–3 mm excised from coronal sutures. A schematic diagram of the mouse calvaria and the area from which the specimens were excised is shown in Fig. 1A. Specimens were placed in a modified polystyrene Petri dish with serum-free media containing DMEM, pH ~7.4, 1 μg/ml gentamicin, 2 mM

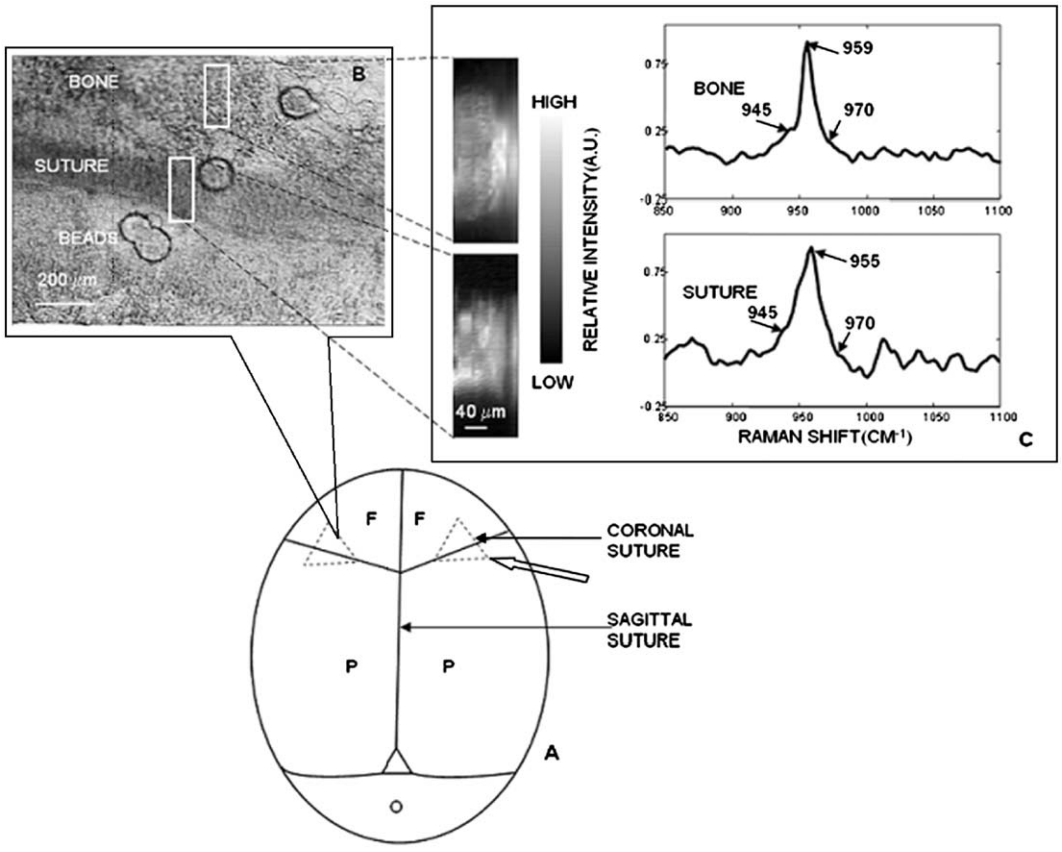

Fig. 1. (A) Schematic diagram of the mouse calvaria and the area from which the specimens were excised: F—frontal bone, P—parietal bone, O—occipital bone. An area containing the coronal suture and frontal and parietal bone tissue is harvested from the calvaria (arrow) at fetal day 18.5. (B) Brightfield image showing control specimen at $t = 0$. The white boxes indicate the areas imaged from mineralized tissue and suture regions. (C) The mineral factors obtained for control specimen from mineralized tissue and suture region, respectively, together with their score image. The image dimensions are ~850 × 120 ($H \times W$) μm.

glutamine, 1 mM non-essential amino acids, 1 mM ITS+ (BD Biosciences, Bedford, MA) and 3 mM inorganic phosphate. The pH in the medium was monitored visually by noting the color of the phenol red indicator. The serum-free medium in these experiments contains about 3×10^{-3} M inorganic phosphate, which served as the only phosphate source for tissue mineralization in the absence of organic phosphates such as triglycerophosphate.

Six calvarial explants were divided into two groups: control empty beads and experimental (FGF2-soaked acrylic bead). Heparin acrylic beads, with a 200–250 μm diameter (Sigma Aldrich Corporation, St. Louis, MO), soaked with recombinant human FGF2 were placed on three calvaria. Empty beads were used as controls for three calvaria. The beads were implanted with a capillary pipette on the osteogenic fronts (OFs) of the coronal sutures. The explants were subsequently cultured at 37°C in a humidified atmosphere of 5% CO_2 in air for 72 h in serum-free medium as described above. When necessary, additional serum-free media was injected into the Petri dishes via the dish septum.

Raman microspectroscopy

Raman spectra were obtained in the imaging Raman microprobe used in earlier studies [27,37]. The excitation wavelength was 785 nm. The laser line was focused onto the specimen through a 5×/0.25 NA objective (Zeiss Fluar, Zeiss, Thornwood, NY) producing incident laser power of ~250–300 mW distributed over a line approximately 850 μm long. Raman scatter was collected through the same microscope objective and focused into an axial-transmissive spectrograph (Kaiser Optical Systems Inc., Ann Arbor, MI; Holospec f/1.8I) equipped with a 50-μm slit, providing a maximum spectral resolution of 6–8 cm^{-1}. Forty lines of Raman spectra spaced 3.1 μm apart (6.2 μm spatial resolution) were acquired, yielding low definition images that provided an ~850 × 120 ($H \times W$) μm field of view. The total acquisition time for each time point was 86 min, with an integration time of 120 s per frame. The elapsed time between specimen preparation and the initiation of $t = 0$ Raman measurements never exceeded 5 min. The irregular location patterns of the beads on the calvaria were used for image registration to ensure that the Raman spectra were obtained at the same location in a specimen every time point (Fig. 2).

Data analysis

Multivariate data analysis

Data analysis was performed in Matlab (Math Works, Inc., Natick, MA) for all spectral images taken from six specimens. The methods used are the same as we have employed in other recent bone tissue studies and will only be summarized here [24,27].

All spectra were preprocessed by removing detector-generated artifacts (spikes) and subtracting the detector dark current. The extraction of Raman spectra was performed by band target entropy minimization (BTEM) [28–32]. BTEM recovers individual chemical component spectra from large sets of spectra of component mixtures. The first step is principal component analysis (PCA) to extract the eigenvectors that describe the original data set. Bands in non-noise eigenvectors (identified by scree plot analysis or other standard tests) that would normally be used for recovery of spectra are examined for localized spectral features. For a targeted (identified) band, information entropy minimization is used to recover the spectrum containing this band and all correlated bands. In addition to the non-noise eigenvectors, the next 5–30 eigenvectors, in which noise predominates, are used in the minimization to improve the signal/noise ratio for minor components. Non-negativity and band shape are used as constraints that define a physically meaningful solution. The recovered spectra (often called factors) describe the original spectral signatures of the various tissue components. The reconstructed data set was considered adequate when the percentage error between the original data set and the reconstructed data was below 5%. In most cases, the reconstructed data set differed from the original data set by less than 1%.

Univariate data analysis

The recovered factors were then subjected to curve fitting and background subtraction (GRAMS/AI (Thermo Galactic, Inc., Salem, NH) to resolve overlapped bands. The recovered factors ride on a small amount of background that was removed by fitting background-only regions of the spectrum to a cubic or quartic function and subtracting. The fitted peaks were mixed (50/50) Gaussian and Lorentzian functions. Peaks were considered fitted when the solution converged with an R^2 value of 0.99 or greater.

To better understand the time course of the composition changes of the newly formed mineral, we examined phosphate band component areas, total integrated phosphate envelope and carbonate band areas. The phosphate ν_1 band envelope in bone mineral is asymmetric and consists of closely spaced incompletely resolved bands. In fitting the phosphate ν_1 envelope, three underlying bands were used, 945 cm^{-1} (ACP), 955 cm^{-1} (OCP), 957–962 cm^{-1} (carbonated apatite) and 970 cm^{-1} (OCP, lit 966–967) [9,19]. In addition, we have included bands at 980–985 cm^{-1} that are observed in the osteogenic front. The carbonate band at 1065–1075 cm^{-1} (carbonate ν_1, phosphate ν_3) is fitted with a single band, although there is evidence that this band is a composite resulting from accidental overlap between ν_1 CO_3^{2-} band and the ν_3 PO_4^{3-} band [33,34].

Band width and band area measurements were made on the recovered spectral factors. Area ratios are reported relative to the area of the most intense phosphate ν_1 component in the 955–962 cm^{-1} range. These area ratios are used as measures of carbonate/phosphate content, amorphous (disordered) calcium phosphate/OCP and amorphous (disordered) mineral/apatitic mineral. The average and standard deviation is calculated at each time point for the control specimens and the FGF2-treated specimens. A t test was used to evaluate the significance of differences in results between FGF2-treated and untreated specimen groups. Differences were considered statistically significant when $P \leq 0.05$.

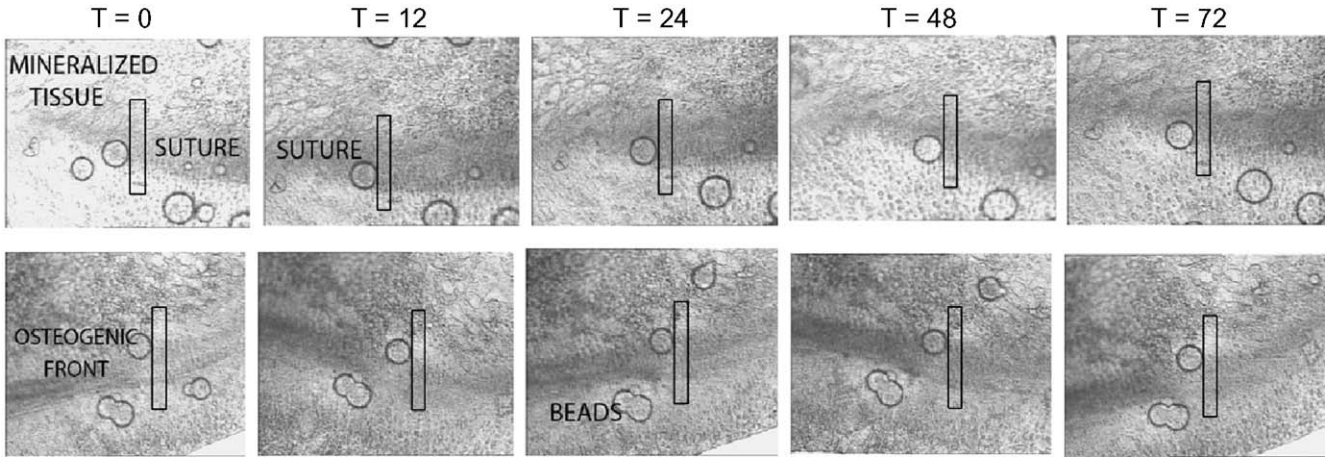

Fig. 2. Brightfield images of empty bead (upper panel) and FGF2-soaked heparin acrylic bead (lower panel) specimens showing progress of mineralization. Mineralization appears as darker shades. The boundaries of Raman-imaged regions are shown as black rectangles.

Results

Fig. 1 shows the area from which the tissue specimens were harvested (Fig. 1A) and the suture and mineralized tissue areas from which the spectra were collected (Fig. 1B). In Fig. 1C, the mineral Raman spectra from the suture and mineralized tissue regions are shown together with the score images that map each mineral distribution. The exact tissue regions imaged are denoted by boxes in Fig. 1B.

The time evolution of a series of unstained specimens treated with FGF2-soaked beads (lower panel) and control specimens treated with empty beads (upper panel) is shown in Fig. 2. The darker color of the lower panels and especially the more sharply defined suture boundaries in the later time periods suggest that FGF2 does cause increased mineralization. Use of the bead pattern for image registration was successful because most beads did not change position over time. Small changes in a few bead positions or even the occasional damaged bead did not hinder registration.

Visual observation showed that phenol red remained red/orange throughout each experiment, confirming that the pH always remained near pH 7.4. Furthermore, to test the hypothesis that formation of OCP or a similar mineral was formed in the growth medium independently of bone tissue matrix, we examined the growth media for precipitated solids prior to using it and found none. These control experiments show that mineral formation is not an artifact of precipitation from the culture medium caused by the presence of inorganic phosphate or by pH change.

In reporting information about mineral phases, we use the names or abbreviations of reference minerals, such as OCP, as convenient designations. That the biomineral phases are not truly stoichiometric minerals is treated in detail in the Discussion section.

For the first 12 h, no difference was found between the spectra of calvaria treated with FGF2 and controls. Fig. 3A shows a representative spectrum taken at the beginning of an experimental sequence. The initial time point spectra were characterized by a low phosphate ν_1 frequency, 955 cm^{-1} (OCP), a prominent shoulder at 945 cm^{-1} (ACP) and a small band around 970 cm^{-1} (OCP). Most workers show, but do not always report, a shoulder at 945–953 cm^{-1}. We can find no previous reports of a band at 970 cm^{-1} in bone tissue. In addition, the full width half height (FWHH) of the 955 cm^{-1} band is broader than is typical in mature tissue. A small carbonate band (not shown) is observed at 1072 cm^{-1}. By contrast, the phosphate ν_1 in mature tissue is found at 957–959 cm^{-1} (Fig. 1C). Associated with the 955 cm^{-1} band, there is a weak band at 1010–1014 cm^{-1} (Fig. 3B). This band is more readily observed after 12 h because the mineral spectra are more intense than at $t = 0$. Fowler et al. consider this to be the most characteristic OCP Raman band [19]. The evolution of deposited mineral from a transient phase (OCP-like) to a more stable phase (carbonated apatite-like) for FGF2-treated specimens is shown in Fig. 3B.

The time courses of mineral bands (factors) for three different control (empty bead) tissue specimens and three FGF2-treated specimens are shown in Figs. 4A–C and in D–F, respectively. The band positions for each specimen at different time points (0, 12, 24, 48, 72 h) are summarized in Table 1B. The patterns are similar, but the early-time features are more prominent in the more rapidly mineralizing FGF2-treated specimens. In general, the main phosphate band moves toward higher frequency, from about 955 cm^{-1} to as high as 962 cm^{-1} over the 72-h period, indicating bone mineral maturation. The shoulder at 945 cm^{-1} (ACP) becomes less prominent after 24 h in the controls but remains prominent in the FGF2-treated specimens. This is because more young, disordered mineral is deposited in specimens undergoing an increased rate of FGF2-induced mineralization. FGF2 increases the rate of mineral deposition [23]. Once the solid is first formed, it is transformed to the final stable phase at a rate that is independent of FGF2. Similarly, the medium intensity OCP band at 970 cm^{-1} becomes less prominent or disappears in most control specimens after 12–24 h but remains prominent in the

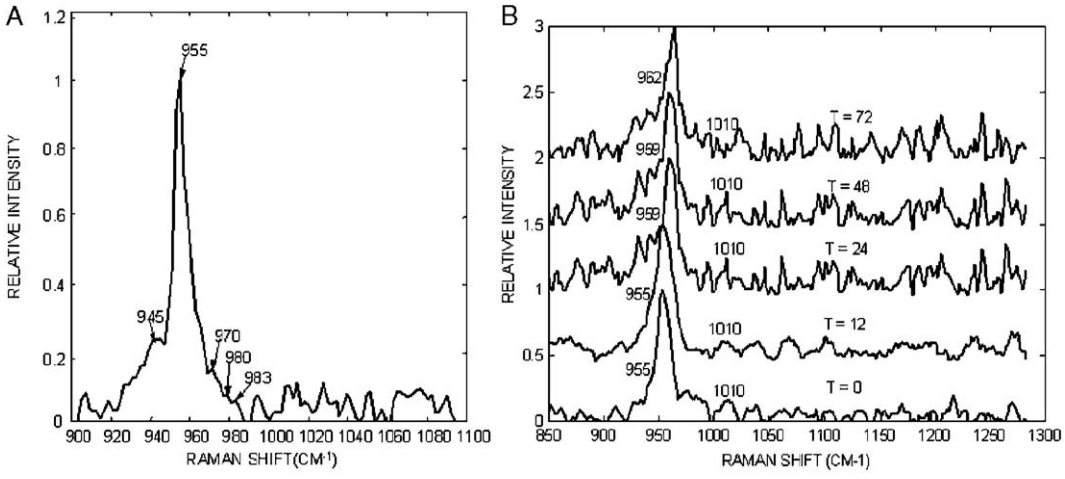

Fig. 3. (A) Raman spectrum (suture region) of specimen treated with an empty bead, 0 h. (B) Raman spectra (suture region) of FGF2-treated specimen over a 72-h period. OCP-like bands at 955, 1010 cm^{-1} are prominent until $t = 24$ h.

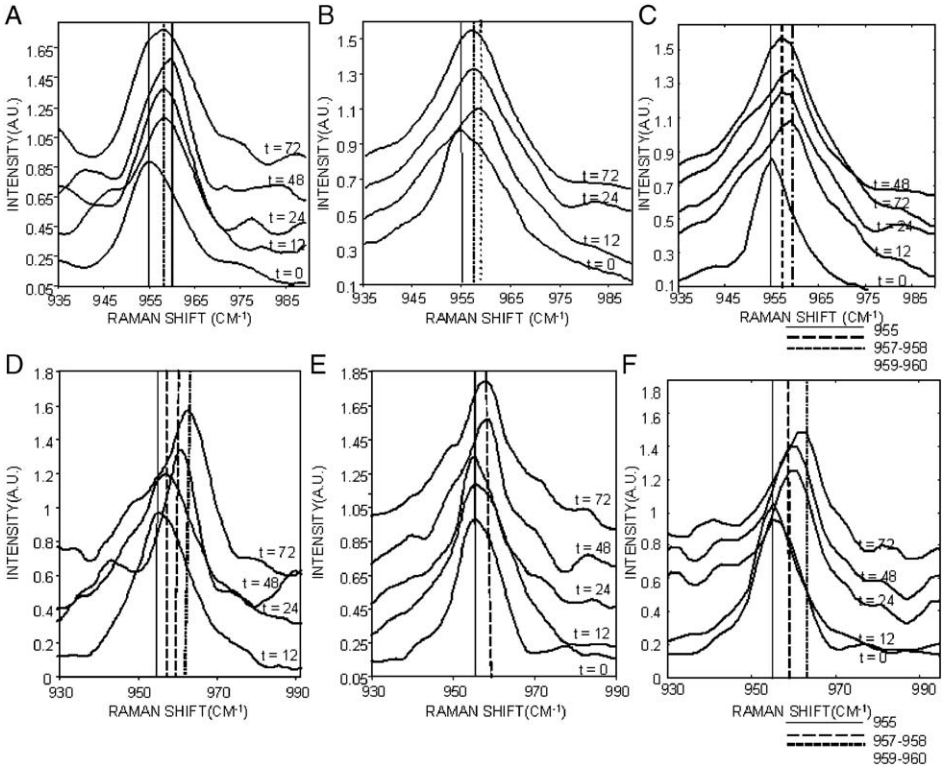

Fig. 4. Plots of the phosphate ν_1 envelope of the Raman spectrum of the control coronal sutures (upper panel, A–C) and FGF2-treated coronal sutures (lower panel, D–F) at different time points for three different tissue specimens.

calvaria treated with FGF2, even at 72 h. In some calvaria, we observed weak bands at 980–985 cm^{-1} (Fig. 3A) and sometimes an OCP band at 1010–1014 cm^{-1} (Fig. 3B), which are Raman signatures for transient intermediates that coexist in the very early phase of mineralization. The presence of a monohydrogen phosphate P–O stretch at 980–985 cm^{-1} suggests that other phosphate phases besides OCP and ACP may be transiently present. Sauer et al. [9] report a dicalcium phosphate dihydrate band at 985 cm^{-1}. However, our data are insufficient to assign these bands definitively to phases that are identical or similar to any phosphate reference mineral.

In Figs. 5 and 6, data for the empty bead controls and FGF2-treated specimens are presented. Band area ratios are used because they are independent of illumination intensity or signal collection efficiency. Band areas are ratioed to the area of the most intense phosphate ν_1 component at 955–962 cm^{-1}.

In the control specimens, the 945:957 cm^{-1} band area ratio initially increases between $t = 0$ and $t = 12$ h. This ratio then decreases irregularly for the remaining time points. A similar trend is found for the 970:957 cm^{-1} band area ratio. In fact, the 970 cm^{-1} band completely disappears after $t = 12$ h. Aside from the $t = 48$ h time point, the 1065:957 cm^{-1} band area ratio (CO_3/PO_4 ratio) decreases as time progresses.

In calvaria treated with FGF2, a somewhat different pattern is observed (Fig. 6). At later time points ($t \geq 24$ h), the areas of the smaller components are a larger fraction of the area of the most intense band component at 955–962 cm^{-1} than is observed for the controls. The 945:957 cm^{-1} band area ratio is initially small at $t = 0$ and $t = 12$ h and increases for the remaining time points. A similar trend is found for the 970:957 cm^{-1} band area ratio. The 970 cm^{-1} band is not observed at $t = 0$ h, and the band area ratio increases irregularly over time. The 1065:957 cm^{-1} band area ratio increases with time from $t = 0$ to $t = 72$ h. Overall, the band area ratio trends for the FGF2-soaked bead specimens are almost the opposite of those observed for the empty bead specimens.

Discussion

It is not completely valid to identify bone mineral with synthetic or natural phosphate minerals. Bone mineral contains varying amounts of cations (e.g., Na^+, K^+ Mg^{+2}) and anions (CO_3^{-2}, Cl^-, F^-). The stable bone mineral is often called hydroxyapatite (HAP) in the bone tissue literature. However, the B-type carbonated apatite, a better model for bone mineral, is called dahllite in the mineralogy literature, and HAP is used only for the uncarbonated mineral. Even these names refer to calcium salts that do not contain ions such as halides or alkalis. Similarly, the transient calcium phosphates such as OCP that have been postulated as precursors to the final, most stable bone mineral, do not contain the substituents that characterize the biomineral [35]. Typically, chemists prepare minerals for spectroscopic or crystallographic study under carefully controlled conditions that are designed to minimize the inclusion of ions other than those comprising the pure mineral. Nonetheless, the reference minerals are convenient shorthand descriptions for

Table 1

A. Assignments for Raman bands of bone tissue components

Raman shifts (cm^{-1})	Band assignment	Component
578–580	ν_4PO_4, ν_4HPO_4	OCP [9,19]
879	HPO_4 (5) [P-(OH)]	OCP [19]
945–952	PO_4, P–O	ACP [9]
955	ν_1 PO_4, P–O	OCP[19]
957–962	ν_1PO_4, P–O	Carbonated apatite
970	ν_1PO_4, P–O	OCP[19]
980–985	P–O stretch, HPO_4	DCPD [9]

B. Plots of the Raman shift (cm^{-1}) of PO_4 ν_1 envelope at different time points for three specimens

Time (hours)		0	12	24	48	72
Control specimens	A	955	957	957	959	957
	B	955	960	958	–	958
	C	955	959	957	959	957
FGF2-treated specimens	A	955	955	958	960	962
	B	955	955	955	959	959
	C	955	955	959	959	962

crystallite structures that may be similar, although not identical, to those of the synthetic materials.

The spectra reported in this study were obtained at approximately 8 cm^{-1} resolution (4 cm^{-1}/pixel, 50 μm slit). However, the peak position of a Raman band can be estimated to a small fraction of a (0.2–0.02 pixel) of a pixel width by fitting the band to a Gaussian/Lorentzian shape [36]. The results of fits are used to assign band positions. Even if the accuracy of the fit is no better than 0.1 pixel, the reported peak position is still accurate to about 0.4 cm^{-1}. Our spectrograph is calibrated against a neon discharge lamp.

The calibration procedure used in our laboratory should be accurate to about 0.1 cm^{-1} [36]. Even if there are small systematic errors in our calibration, they are the same through the measurements and do not affect reported *changes* in Raman

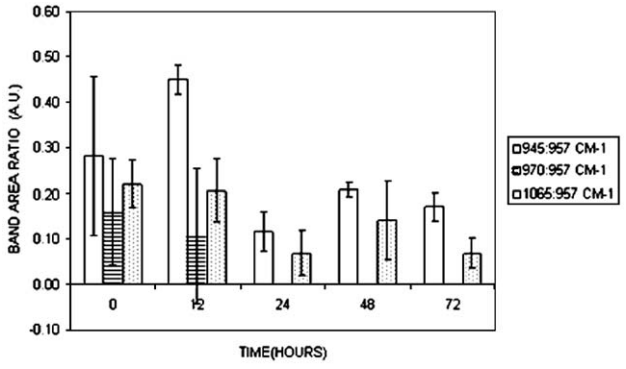

Fig. 5. Band area ratios of the Raman mineral bands for control specimen suture regions as a function of time. The ratios are calculated for each of the three specimens and then averaged. Errors bars are ±1 standard deviation.

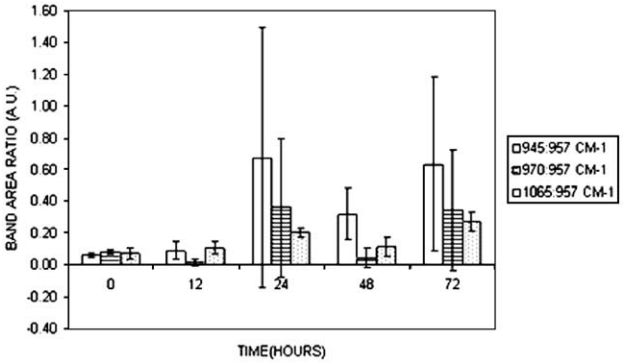

Fig. 6. Band area ratios of the Raman mineral bands for FGF2-soaked bead specimen suture regions as a function of time. The ratios are calculated for each of the three specimens and then averaged. Errors bars are ±1 standard deviation.

band positions. Therefore, it is reasonable to attribute a 2 cm^{-1} change in the position of phosphate ν_1, the most intense band in the bone mineral spectrum, to a change in the phosphate-containing mineral phase. Because bone mineral is not a pure stoichiometric compound, it is not valid to assume that phosphate ν_1 will be found at exactly the same cm^{-1} position in every bone tissue specimen. Similarly, we are reluctant to attribute significance to small changes in the weaker mineral bands because these are observed at low signal/noise ratio in the early stages of mineralization.

Because Raman microspectroscopy and imaging were always performed through the silica viewing window of a sealed Petri dish, the tissue remained viable despite the periodic examination at room temperature (20–22°C). Development probably was slowed during these times of reduced temperature. Exposure to 785-nm radiation causes no photochemical changes, but heating could be a concern. Our specimens were kept in Petri dishes filled with serum-free medium, and so part of the heat was dissipated to the surrounding water, which is a good thermal conductor. We have previously studied 785 nm laser heating effect in Raman microscopic imaging of stained and unstained bone tissue. In that work, we could observe no damage to tissue stained with eosin or toluidine blue, but we did find laser-induced thermal damage to tissue heavily stained with hematoxylin [37]. Even that damage could be eliminated with a modified staining protocol resulting in less stain deposited in the tissue.

It is also known that elevated phosphate or calcium can induce mineralization in many tissues. Yang and co-workers have recently used mineralization of smooth muscle cells in vitro in the presence of excess calcium or phosphate as a model for vascular calcification [38]. However, the process is slow in the culture medium, whose phosphate serves mostly to prevent dissolution of mineral.

In this study, we have found evidence for transient mineral phases. These transient intermediates have not been reported previously because other workers have used tissue sampling and preparation protocols that preceded spectroscopic measurement by sufficient time to allow transformation the thermodynamically most stable phases to occur, reducing the likelihood of finding an unstable species.

The band at 945 cm^{-1} has been observed for amorphous calcium phosphate [9] and is indicative of a highly disordered structure, although not necessarily a completely amorphous one. In keeping with this assignment, this band becomes less prominent as the mineral ages and is often observed to shift to higher frequency as well.

Surprisingly, we do see a phosphate ν_1 955 cm^{-1} band that is attributable to an OCP-like mineral. Associated with it is a 1010 cm^{-1} band that is a P–O stretch of monohydrogen phosphate and is also found in OCP [9,19]. The 955 cm^{-1} band in the FGF2-treated specimens is almost always accompanied by a shoulder around 970 cm^{-1}. Fowler and co-workers [19] report changes in OCP bands as a function of laser power ($\lambda = 488$ nm). Sauer and co-workers [9] report that OCP has an intense band at 957 cm^{-1} but that, if the crystals are tightly packed and the laser power ($\lambda = 1.064$ μm) is increased to 150 mW, the band can be resolved into a doublet with components at 956 cm^{-1} and 967 cm^{-1}. It is difficult to know where to place our experiments in these power regimes. Our microscope spreads the laser beam into a high aspect ratio rectangle that minimizes local power density. The crystallites are in a predominantly aqueous medium, suggesting that our observations are made under low power conditions. With allowance for inclusion of other cations or anions, our early time spectra demonstrate the presence of an OCP-like mineral and possibly even a phase similar to β-TCP.

In the control specimens (empty bead), the phosphate ν_1 band is at 955 cm^{-1} for $t = 0$ h only. After this time point, the phosphate ν_1 band shifts 2 cm^{-1} to 957 cm^{-1}, close to the 957–958 cm^{-1} reported for phosphate ν_1 in most previous studies (Figs. 4A–C). This is not the case for the FGF2-treated specimens. The spectra of these calvaria show the 955 cm^{-1} phosphate ν_1 band for at least another 12 h (Figs. 5A–C). This could be the consequence of the perturbation of the normal physiological process when FGF2 is added to the calvarial tissue. However, FGF2-induced mineral deposition is not an immediate response because the factor must diffuse from the beads to the tissue and also because response requires activation of many pathways. These include new protein synthesis, expression of the osteopontin gene, and increased Msx2 expression [14,39,40]. FGF2 alone also enhances mineral deposition in osteoblasts [12]. We have no evidence that FGF2 causes a change in the sequence of reaction that leads to mineralized tissue. Rather, accelerated mineralization induced by FGF2 causes incorporation of more phosphates from the extracellular compartment into unstable mineral species. The rate of conversion of unstable intermediate species to the more mature mineral is unchanged. The addition of FGF2 results in a more rapid and more prolonged formation of matrix and so prolongs the time over which unstable calcium phosphates such as ACP and OCP are spectroscopically observable. Therefore, we are better able to see the evolution of the earliest mineral in the treated specimens than in the controls.

The main ν_1 component of a B-type carbonated apatite (i.e., a dahllite structure) is usually found at 959–962 cm^{-1}. This band is observed first in control tissue specimens that have been cultured for at least 12 h. The presence of a band at 962 cm^{-1} is surprising. A phosphate ν_1 shift to higher frequency is associated with the presence of anions, especially chloride and fluoride, in the apatitic mineral c axis [41]. It is possible that transient incorporation of chloride from the salts in the culture media or the extracellular matrix occurs as one step in the ultimate conversion to a carbonated apatite. A test of this hypothesis requires further experimentation.

We caution that our results are qualitative only. It is well known that consecutive and coupled reactions give rise to complex kinetics and to peculiar time dependences of concentrations of intermediates in a reaction sequence. Only the simplest cases have analytic solutions [42]. The problem is exacerbated when the reaction sequence is coupled to a transport process such as diffusion. In this case, counter-intuitive results, such as movement of reactants from regions of low concentration to regions of higher concentration [43] or self-segregation of reactants [44], often occur. The tissue mineralization considered in this study is especially complex. Several proteins participate in intramembranous ossification, and the mineral product is a solid, not a liquid. The growth factor FGF2 is introduced by diffusion from a spherical reservoir, the diffusion field is convectively perturbed as the specimens are carried between laboratories and diffusion proceeds through an ill-defined thickness of tissue across a second boundary, the tissue surface, that itself does not have a geometrically simple description.

We have been able to follow the temporal evolution of early mineral species deposited in normal and craniosynostotic mineralization over a 3-day period. Because of the complexity of the system, it is not yet possible to provide a quantitative description of the kinetics of progression of the mineral from initially disordered material to carbonated apatite crystallites. Even at this early stage, these experiments provide new information because the suture and osteogenic front is studied as it evolves over this time. Our results may resolve some uncertainties in the tissue mineralization literature. Unless mineralizing tissue is examined spectroscopically almost immediately after it is harvested, the observed mineral will be a carbonated apatite.

Our results also demonstrate that Raman spectroscopy is a powerful tool for examination of bone in a native state. Living tissue is more complex than simple mixtures of inorganic salts or even cell cultures. The tissue is responsible for secreting growth factors and hormones that control tissue function and the mineralization process itself. It is likely that correlative NIR Raman and visible fluorescence spectroscopies of labeled non-collagenous proteins or correlative Raman spectroscopic and immunostaining measurements will be needed to study in detail the interaction of mineral, matrix collagen, of growth factors and hormones. Further spectroscopic study in living tissue should prove valuable in understanding mineralization under physiological and pathological conditions.

Acknowledgments

This research was supported by NIH grants R01 AR047969 (M.D.M.) and R29DE011530 (M.A.I.) and University of Michigan Musculoskeletal Diseases Core Center through NIH P30 AR046024.

References

[1] Weiner S, Sagi I, Addadi L. Choosing the crystallization path less traveled. Science 2005;309:1027–8.

[2] Brown WE. Crystal structure of octacalcium phosphate. Nature 1962;196:1048–50.

[3] Brecevic L, Fuhredi-Milhofer H. Precipitation of calcium phosphates from electrolyte solutions: II. The formation and transformation of the precipitates. Calcif Tissue Res 1972;10:83–9.

[4] Brown WE, Eidelman N, Tomazic B. Octacalcium phosphate as a precursor in biomineral formation. Adv Dent Res 1987;1:306–13.

[5] Lowenstam HA, Weiner S. Transformation of amorphous calcium phosphate to crystalline dahllite in the radular teeth of chitons. Science 1985;227:51–2.

[6] Rey C, Kim H-M, Gerstenfeld L, Glimcher MJ. Structural and chemical characteristics and maturation of the calcium–phosphate crystals formed during the calcification of the organic matrix synthesized by chicken osteoblasts in cell culture. J Bone Miner Res 1995;10:1577–88.

[7] Kuhn L, Xu Y, Rey C, Gerstenfeld L, Grynpas M, Ackerman J, et al. Structure, composition, and maturation of newly deposited calcium-phosphate crystals in chicken osteoblast cell cultures. J Bone Miner Res 2000;15:1301–9.

[8] Sauer GR, Wuthier RE. Fourier transform infrared characterization of mineral phases formed during induction of mineralization by collagenase-released matrix vesicles in vitro. J Biol Chem 1988;263: 13718–24.

[9] Sauer GR, Zunic WB, Durig JR, Wuthier RE. Fourier transform Raman spectroscopy of synthetic and biological calcium phosphates. Calcif Tissue Int 1994;54:414–20.

[10] Johnsson MS, Nancollas GH. The role of brushite and octacalcium phosphate in apatite formation. Crit Rev Oral Biol Med 1992;3:61–82.

[11] Iijima M, Moradian-Oldak J. Control of octacalcium phosphate and apatite crystal growth by amelogenin matrices. J Mater Chem 2004;14:2189–99.

[12] Chaudhary LR, Hofmeister AM, Hruska KA. Differential growth factor control of bone formation through osteoprogenitor differentiation. Bone 2004;34:402–11.

[13] Stewart S, Shea DA, Tarnowski CP, Morris MD, Wang D, Franceschi R, et al. Trends in early mineralization of murine calvarial osteoblastic cultures: a Raman microscopic study. J Raman Spectrosc 2002;33: 536–43.

[14] Ignelzi Jr MA, Wang W, Young AT. Fibroblast growth factors lead to increased Msx2 expression and fusion in calvarial sutures. J Bone Miner Res 2003;18:751–9.

[15] Timlin J, Carden A, Morris MD, Rajachar RM, Kohn DH. Raman spectroscopic imaging markers for fatigue-related microdamage in bovine bone. Anal Chem 2000;72:2229–36.

[16] Timlin JA, Carden A, Morris MD, Bonadio JF, Hoffler CE, Kozloff KM, et al. Spatial distribution of phosphate species in mature and newly generated mammalian bone by hyperspectral Raman imaging. J Biomed Opt 1999;4:28–34.

[17] Mendelsohn R, Hassankhani A, DiCarlo E, Boskey A. FT-IR microscopy of endochondral ossification at 20 μ spatial resolution. Calcif Tissue Int 1989;44:20–4.

[18] Rey C, Kim HM, Gerstenfeld L, Glimcher MJ. Characterization of the apatite crystals of bone and their maturation in osteoblast cell culture: comparison with native bone cells. Connect Tissue Res 1996;35: 343–9.

[19] Fowler BO, Markovic M, Brown WE. Octacalcium phosphate. 3. Infrared and Raman vibrational spectra. Chem Mater 1993;5:1417–23.

[20] Carden A, Morris MD. Application of vibrational spectroscopy to the study of mineralized tissue (review). J Biomed Opt 2000;5:259– 268.

[21] Crane N, Wang W, Ignelzi Jr MA, Morris MD. Spectral imaging of mouse skull undergoing craniosynostosis. SPIE Proc 2003;4959:111– 119.

[22] Morris MD, Stewart S, Tarnowski C, Shea D, Franceschi R, Wang D, et al. Raman spectroscopy of early mineralization of normal and pathological calvaria. SPIE Proc 2002;4614:28–39.

[23] Tarnowski CP, Ignelzi Jr MA, Morris MD. Mineralization of developing mouse calvaria as revealed by Raman microspectroscopy. J Bone Miner Res 2002;17:1118–26.

[24] Crane N, Yu G, Ignelzi Jr MA, Morris M. Study of localization of response to fibroblast growth factor-2 in murine calvaria using Raman spectroscopic imaging. SPIE Proc 2004;5321:242–9.

[25] Iseki S, Wilkie AOM, Morriss-Kay GM. Fgfr1 and Fgfr2 have distinct differentiation- and proliferation-related roles in the developing mouse skull vent. Development 1999;126:5611–20.

[26] Wu Y, Ackerman JL, Strawich ES, Rey C, Kim HM, Glimcher MJ. Phosphate ions in bone: identification of a calcium-organic phosphate complex by 31P solid-state NMR spectroscopy at early stages of mineralization. Calcif Tissue Int 2003;72:610–26.

[27] Crane NJ, Morris MD, Ignelzi Jr MA, Yu GG. Raman imaging demonstrates FGF2-induced craniosynostosis in mouse calvaria. J Biomed Opt 2005;10(3):031119.

[28] Widjaja E, Li C, Chew W, Garland M. Band-target entropy minimization. a robust algorithm for pure component spectra recovery. Application to complex randomized mixtures of six components. Anal Chem 2003; 75:4499–507.

[29] Widjaja E, Crane N, Chen T, Morris MD, Ignelzi Jr MA, McCreadie B. Band-target entropy minimization (BTEM) applied to hyperspectral Raman image data. Appl Spectrosc 2003;57:1353–62.

[30] Wee C, Widjaja E, Garland M. Band-target entropy minimization (BTEM): an advanced method for recovering unknown pure component spectra. Application to the FTIR spectra of unstable organometallic mixtures. Organometallics 2002;21:1982–90.

[31] Ong LR, Widjaja E, Stanforth R, Garland M. Fourier Transform Raman spectral reconstruction of inorganic lead mixtures using a novel band-target entropy minimization (BTEM) method. J Raman Spectrosc 2003;34:282–9.

[32] Sin S, Widjaja E, Yu L, Garland M. Application of FT-Raman and FTIR measurements using a novel spectral reconstruction algorithm. J Raman Spectrosc 2003;34:795–805.

[33] Penel G, Leroy G, Rey C, Bres E. MicroRaman spectral study of the PO4 and CO3 vibrational modes in synthetic and biological apatites. Calcif Tissue Res 1998;63:475–81.

[34] Penel G, Delfosse C, Descamps M, Leroy G. Composition of bone and apatitic biomaterials as revealed by intravital Raman microspectroscopy. Bone 2005;36:893–901.

[35] Mathai M, Shozo T. Crystal structures of calcium orthophosphates. In: Chow LC, Eanes ED, editors. Octacalcium Phosphate. Gaithersburg, MD: Karger; 2001. p. 1–16.

[36] Mann CK, Vickers TJ. The quest for accuracy in Raman spectra. In: Lewis IR, Edwards HGM, editors. Handbook of Raman Spectroscopy: From the Research Laboratory to the Process Line. New York, NY: Marcel Dekker, Inc.; 2001. p. 251–74.

[37] Morris M, Crane N, Gomez L, Ignelzi Jr MA. Compatibility of staining protocols for bone tissue with Raman imaging. Calcif Tissue Int 2004;74:86–94.

[38] Young H, Curinga G, Giachelli CM. Elevated extracellular calcium levels induce smooth muscle cell matrix mineralization in vitro. Kidney Int 2004;66:2293–9.

[39] Iseki S, Wilkie AOM, Heath JK, Ishimaru T, Eto K, Morriss-Kay GM. Fgfr2 and osteopontin domains in the developing skull vault are mutually exclusive and can be altered by locally applied FGF2. Development 1997;124:3375–84.

[40] Kim HJ, Lee MH, Park HS, Park MH, Lee SW, Kim SY, et al. Erk pathway and activator protein 1 play crucial roles in FGF2-simulated premature cranial suture closure. Dev Dyn 2003;227:335–46.

[41] Pasteris JD, Wopenka B, Freeman JJ, Rogers K, Valsam-Jones E, van der Houwen JAM, et al. Lack of OH in nanocrystalline apatite as a function of degree of atomic order: implications for bone and biomaterials. Biomaterials 2004;25:229–38.

[42] Cox BG. Modern Liquid Phase Kinetics. Oxford: Oxford Univ. Press; 1994. p. 23–41.

[43] Sheu W-S, Lindenberg K, Kopelman R. Scaling properties of diffusion-limited reactions. Phys Rev, A 1990;47:2279–83.

[44] Morris MD. Contribution of electrostatic coupling to electrical migration. In chronopotentiometry. J Electroanal Chem 1964;8:1–4.